


Write-Error Reduction of Voltage-Torque-Driven Magnetization Switching by a Controlled Voltage Pulse

Tatsuya Yamamoto,^{1,*} Takayuki Nozaki,¹ Hiroshi Imamura,¹ Yoichi Shiota,^{1,†} Takuro Ikeura,^{1,2} Shingo Tamaru,¹ Kay Yakushiji,¹ Hitoshi Kubota,¹ Akio Fukushima,¹ Yoshishige Suzuki,^{1,3} and Shinji Yuasa¹

¹*National Institute of Advanced Industrial Science and Technology, Spintronics Research Center, Tsukuba, Ibaraki 305-8568, Japan*

²*Graduate School of Pure and Applied Sciences, Tsukuba University, Tsukuba 305-8577, Ibaraki, Japan*

³*Graduate School of Engineering Science, Osaka University, Toyonaka, Osaka 560-8531, Japan*

 (Received 9 August 2018; revised manuscript received 29 November 2018; published 8 January 2019)

We study the effects of pulse shape on the write-error rate (WER) of perpendicularly magnetized magnetic tunnel junctions driven by subnanosecond voltage pulses. The WER almost monotonically increases as the rise time of the write pulse is increased. On the other hand, a small fall time is found to reduce the WER. These experimental results are reproduced well by numerical simulations based on macrospin approximation. The numerical simulations reveal that a proper fall time cancels magnetization drift due to intrinsic damping and that this contributes to the WER reduction. We demonstrate that the magnetization dynamics can be precisely manipulated by a controlled voltage-pulse shape and also show the importance of controlling the pulse shape for achieving a low WER.

DOI: [10.1103/PhysRevApplied.11.014013](https://doi.org/10.1103/PhysRevApplied.11.014013)

I. INTRODUCTION

Voltage-controlled magnetic anisotropy (VCMA) has brought great advances in the ultralow-energy manipulation of magnetization in a wide variety of material systems, including multiferroics [1–4], ferromagnetic ultrathin films [5–7], and ferromagnetic semiconductors [8]. The observation of a large VCMA effect in an Fe/MgO structure [6] is especially important from a practical point of view because this structure is compatible with conventional magnetic tunnel junctions (MTJs), which are the central device of magnetic random-access memories (MRAMs). The VCMA effect in Fe/MgO and related structures can mostly be explained as the sum of selective electron/hole doping in the d -electron orbitals and the induction of a magnetic dipole moment [9–13]. This VCMA mechanism makes it possible to manipulate magnetization under high frequency in the gigahertz regime as has been demonstrated in ferromagnetic resonance experiments [14,15].

The applicability of the VCMA effect has further been broadened by the demonstration of magnetization switching in MTJs by application of subnanosecond pulsed voltage [16,17]. The magnetization switching is driven

by the VCMA-induced effective field change associated with the charge accumulation; this makes it possible to switch a magnetic element within subnanoseconds at an energy cost of less than 10 fJ per bit [18,19]. These properties of voltage-driven magnetization switching are highly beneficial for MRAMs, for which there are growing demands for a high switching speed as well as a low write energy. To develop an energy-efficient voltage-driven MRAM, we necessarily face the problem of high write-error rate (WER). In previous work we achieved a WER of 4×10^{-3} in perpendicularly magnetized MTJs (PMTJs) consisting of a MgO/Fe₈₀B₂₀/W structure [20]. We then achieved a reduced WER of 2×10^{-5} in PMTJs consisting of a Ta/(Co₃₀Fe₇₀)₈₀B₂₀/MgO structure [21]. Experimental results obtained in this work show that the WER can be reduced by increase of the thermal stability factor $\Delta = K_u \mathcal{V} / k_B T$ (where K_u is the uniaxial magnetic anisotropy constant, \mathcal{V} is the volume of the magnet, k_B is the Boltzmann constant, and T is temperature) of the magnetic free layer as well as the magnitude of the VCMA effect.

However, there might be an alternative way of reducing the WER (e.g., by controlling the write pulse shape). Since voltage-driven magnetization switching is mediated by VCMA-induced ultrafast control of the perpendicular magnetic anisotropy, the WER is sensitive to the write pulse width and the pulse amplitude [20,21]. Very recently, it was revealed that the pulse width affects the

*yamamoto-t@aist.go.jp

†Present address: Institute for Chemical Research, Kyoto University, Uji, Kyoto, 611-0011, Japan

transition probability of magnetization between the precession orbitals induced by thermal fluctuation [22]. In the aforementioned studies, the effects of pulse width and amplitude on the WER were investigated in detail; however, the relationships between the WER and other principal pulse parameters such as the rise time (t_{rise}) and the fall time (t_{fall}) have yet to be addressed. In the current work, we study the effects of voltage-pulse shape on the WERs of PMTJs by systematically varying t_{rise} and t_{fall} as well as the duration of the write voltage pulse (t_{pulse}). We find that the WER monotonically increases as t_{rise} increases, whereas it decreases with a moderate t_{fall} . We use numerical simulations to ascertain the effects of pulse shaping on the WER.

II. EXPERIMENT

We measure the WER using a PMTJ and the microwave circuit illustrated in Fig. 1(a). The multilayered film of Ta(5 nm)/(Co₃₁Fe₆₉)₈₀B₂₀(1.1 nm)/MgO(1.4 nm)/(Co₁₀Fe₉₀)₈₀B₂₀(1.4 nm) is prepared on a chemical-mechanical-polished Si substrate with a bottom electrode with use of a sputtering system (Canon ANELVA EC7800). The magnetization direction of the (Co₁₀Fe₉₀)₈₀B₂₀ layer is fixed by a (Co/Pt)-based perpendicularly magnetized synthetic antiferromagnetic layer. The whole stack is deposited at room temperature and is *ex situ* annealed in a vacuum at 250 °C for 1 h. The film is then microfabricated into circular PMTJs with a diameter of approximately 80 nm by conventional techniques, including electron-beam lithography, photolithography, and Ar-ion etching. More details on the microfabrication process can be found elsewhere [21,22]. The resistance values of the PMTJs are typically approximately 200 kΩ for the parallel-magnetization configuration and approximately 350 kΩ for the antiparallel-magnetization configuration. Voltage pulses with various t_{pulse} , t_{rise} , and t_{fall} values are generated by an arbitrary-waveform generator (AWG) with an analog bandwidth of 25 GHz (Keysight M8195A) and fed into a PMTJ through the rf port of the bias tee after being amplified by a preamplifier. The microwave circuit and the PMTJ are connected with a microwave probe. Because of the impedance mismatch, the amplitude of the pulse voltage (V_{pulse}) almost doubles at the end of the PMTJ compared with that at the (impedance-matched) oscilloscope. This is confirmed from a calculation that takes into account the signal transmission and reflection at each circuit component (e.g., bias tee, PMTJ, and rf probe) as reported in Ref. [23]. The PMTJ is dc-voltage biased and the magnetization configuration (either parallel or antiparallel magnetization) is monitored with a real-time oscilloscope. When the dc source is set to -200 mV, the dc voltage at the end of PMTJ is estimated to be approximately -45 mV, which is about 50 times smaller than the voltage required to induce magnetization switching. It was confirmed from a separate measurement

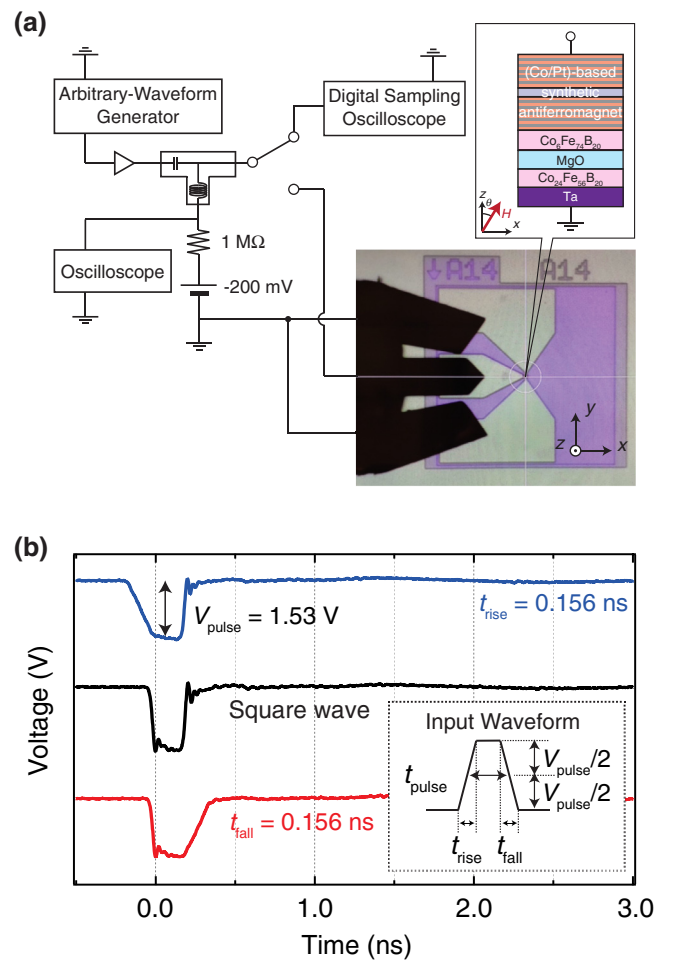


FIG. 1. (a) A PMTJ along with a microwave circuit used for evaluating the WER. The PMTJ consists of a Ta(5 nm)/(Co₃₁Fe₆₉)₈₀B₂₀(1.1 nm)/MgO(1.4 nm) free layer and a 1.4-nm-thick (Co₁₀Fe₉₀)₈₀B₂₀ reference layer with a (Co/Pt)-based synthetic antiferromagnetic layer. The static magnetic field H applied during measurements has a polar angle θ from the perpendicular axis (z axis). (b) Voltage-pulse shapes after amplification. The inset provides definitions of t_{pulse} , t_{rise} , t_{fall} , and V_{pulse} .

that a dc voltage on the order of 10 mV has a negligible influence on the coercivity of the (Co,Fe)B free layer [22], and thereby its contribution to the magnetization switching can be ignored. The oscilloscope and the AWG are synchronized by an external trigger with a frequency of 1 kHz. As necessary, the output waveform from the AWG is checked by a digital sampling oscilloscope equipped with a sampling module with an analog bandwidth of 50 GHz. The WERs are measured under a tilted magnetic field H with polar angle θ , where the in-plane component of H (H_x) determines the precessional axis of the magnetization during t_{pulse} , whereas the perpendicular one (H_z) cancels the stray field from the reference layer and balances the WER of parallel-to-antiparallel and antiparallel-to-parallel

switching. The WERs are calculated from 2×10^4 to 2×10^5 trials depending on t_{pulse} . All the experimental data presented here are obtained from a single representative device, but we obtain similar results from other devices prepared on different wafers.

III. RESULTS AND DISCUSSION

We first check the pulse shape at the end of a rf cable located just before the microwave probe by using the digital sampling oscilloscope. Figure 1(b) displays examples of the measured waveforms. The polarities of the output waves are inverted from those of the input waves since we use an inverting amplifier. Although the AWG inherently possesses a rise and fall time of approximately 0.030 ns, the variation widths of t_{rise} and t_{fall} are almost the same as designed. Therefore, below we discuss the experimental results using nominal values of t_{pulse} , t_{rise} , and t_{fall} for simplicity. The voltage ringing that appears when t_{rise} and t_{fall} are small has a trivial effect on the magnetization dynamics. This is because the frequency of the ringing is about 1 order of magnitude higher (approximately 25 GHz) than the Larmor precession frequency under the measurement conditions (1–3 GHz [22]) and thus the response of magnetization to the voltage ringing is averaged out.

Figures 2(a) and 2(b) display, respectively, the dependence of the WER on t_{pulse} for various t_{rise} and t_{fall} . Dotted black lines represent the data obtained by our applying square pulses ($t_{\text{rise}} = t_{\text{fall}} = 0$ ns). These measurements are performed at $H = 1030$ Oe and $\theta = 68^\circ$, which yields $H_x \sim 970$ Oe and $H_z \sim 350$ Oe. V_{pulse} is set to 1.53 V. Although the displayed WER is for one of the two polarities (i.e., parallel-to-antiparallel or antiparallel-to-parallel-switching) whichever WER is higher, a similar trend is

observed for both polarities. Regardless of t_{rise} and t_{fall} , the WER exhibits a minimum around $t_{\text{pulse}} = 0.2$ ns, which corresponds to half the period of magnetization precession [16,17]. The local maximum in the WER visible around $t_{\text{pulse}} = 0.15$ ns is related to the thermally induced transition of magnetization between precession orbits during the relaxation process [22]. Several definite changes appear in the WER on our increasing t_{rise} and t_{fall} . First, the minimum value of the WER gradually increases as t_{rise} increases. Second, in contrast to the case of t_{rise} , the minimum value of the WER is substantially reduced when $t_{\text{fall}} \sim 0.15$ ns is applied. However, a further increase in t_{fall} gives rise to an increasing minimum value of the WER.

Below we discuss the experimental results by comparing them with the results of numerical simulations based on the macrospin model. We solve the Landau-Lifshitz-Gilbert equation:

$$\frac{d\mathbf{m}}{dt} = -\gamma \mathbf{m} \times \mathbf{H}_{\text{eff}} + \alpha \mathbf{m} \times \frac{d\mathbf{m}}{dt}, \quad (1)$$

where \mathbf{m} is the magnetization unit vector, t is the time, α is the damping constant, and \mathbf{H}_{eff} is the effective field given by

$$\mathbf{H}_{\text{eff}} = -\frac{1}{M_s} \frac{dE}{d\mathbf{m}}, \quad (2)$$

where M_s the saturation magnetization, and E is the energy density expressed as

$$E = K_u(1 - m_z^2) - M_s H_x m_x. \quad (3)$$

During the voltage pulse, $K_u = 0$ is assumed; this allows the magnetization in the ferromagnet to precess

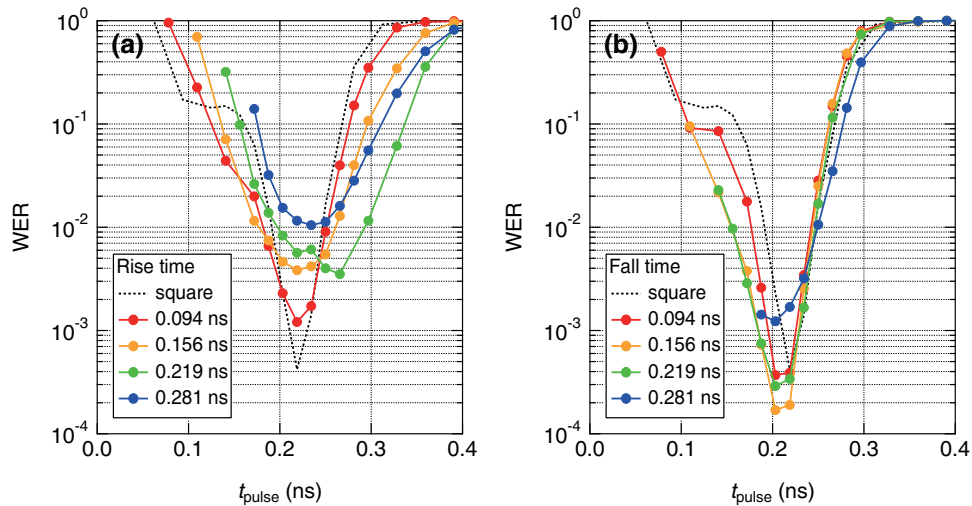


FIG. 2. WER as a function of t_{pulse} with various values of t_{rise} (a) and t_{fall} (b). Dotted black lines represent data obtained with square pulses.

around H_x . The following values are used as material parameters: $\alpha = 0.1$, $K_u = 1.1 \times 10^6$ erg/cm³, $M_s = 955$ emu/cm³ [21], and $\mathbf{H} = H_x = 970$ Oe. The thermal effects are included by our introducing a thermal agitation field [24]. The ferromagnet is assumed to be 40 nm in diameter with a thickness of 1.1 nm. The WERs are calculated from 10^7 trials.

Figure 3 compares the experimental results [Figs. 3(a)–3(d)] with the numerical simulation results [Figs. 3(e)–3(h)]. Although there is a slight offset of t_{rise} and t_{fall} , which may come from the nonzero rise and fall times the AWG intrinsically has, a good correspondence can be seen in the dependence of the WER on t_{pulse} . In the numerical simulations, the minimum value of the WER is reduced by our introducing $t_{\text{fall}} = 0.05$ and 0.1 ns and is increased by our introducing $t_{\text{fall}} = 0.15$ and 0.2 ns. This is in contrast to the case of t_{rise} , where the minimum value of the WER shows only a monotonic increase with increased t_{rise} . It is of great interest that numerical simulations based on a simple macrospin model can reproduce the experimental results. Unlike the cases of spin-transfer-torque- or magnetic-field-driven magnetization switching, where domain-wall nucleation and propagation play an important role, the voltage-torque-driven magnetization switching is initiated by magnetization rotation whose angular velocity is solely determined by the external magnetic field [22]; that is, all the spins in the ferromagnet rotate at the same angular velocity during the voltage application. This means that if we start from a

uniformly magnetized state, the pulsed-voltage application gives rise to a uniform magnetization precession without domain-wall nucleation. Still, domain walls formed in the initial state (i.e., before voltage-pulse application) and/or nonuniformity of the perpendicular magnetic anisotropy as well as the VCMA effect over a junction due to sample imperfection may result in a nonuniform magnetization precession. Such a contribution must be treated micromagnetically and may also become another source of write errors. However, the good correspondence between the experimental results and the simulation suggests that the observed WER change can be qualitatively understood by the use of the macrospin approximation.

To ascertain the origin of the WER reduction, we investigate the magnetization trajectory induced by the pulsed-voltage application. Figure 4 displays the magnetization trajectories superimposed on the magnetic energy contour in the absence of voltage. t_{pulse} is chosen such that it gives a minimum WER at 300 K for each t_{rise} and t_{fall} value. Here ϕ is the azimuth angle from the x direction. The energy density has one saddle point at $m_x = 1$, one energy maximum at $m_x = -1$, and two minima at $\tilde{\mathbf{m}}_{\pm} = (\tilde{m}_x, 0, \pm\sqrt{1 - \tilde{m}_x^2})$ (black dots), where $\tilde{m}_x = M_s H_x / (2K_u)$. The magnetization rotates around H_x during t_{pulse} (red lines), and once the voltage is turned off (orange dots), it starts to relax to $\tilde{\mathbf{m}}_-$ (green lines). These numerical simulations are performed without our including the thermal effect (i.e., at $T = 0$ K), and hence these trajectories are perfectly reproducible for a given initial state and pulse shape. In

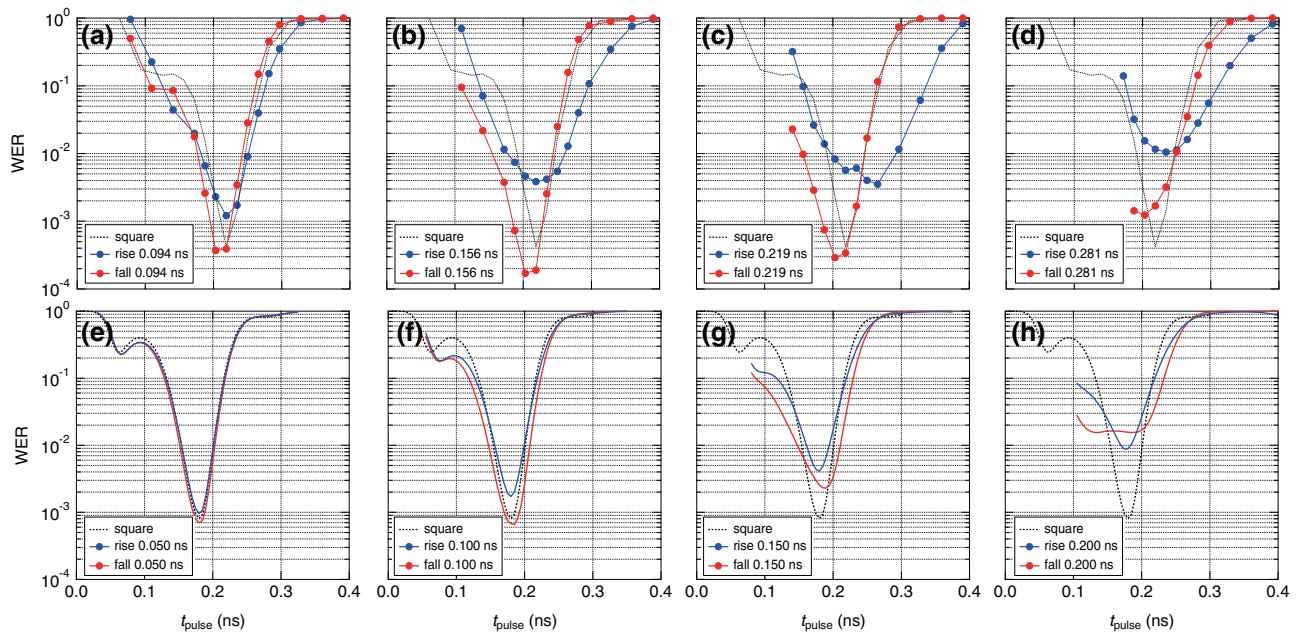


FIG. 3. Effects of t_{rise} and t_{fall} on WER: (a)–(d) experimental results; (e)–(h) numerical simulation results. Blue (red) lines and symbols represent data with $t_{\text{rise}} > 0$ ($t_{\text{fall}} > 0$). Dotted black lines represent data obtained with square pulses.

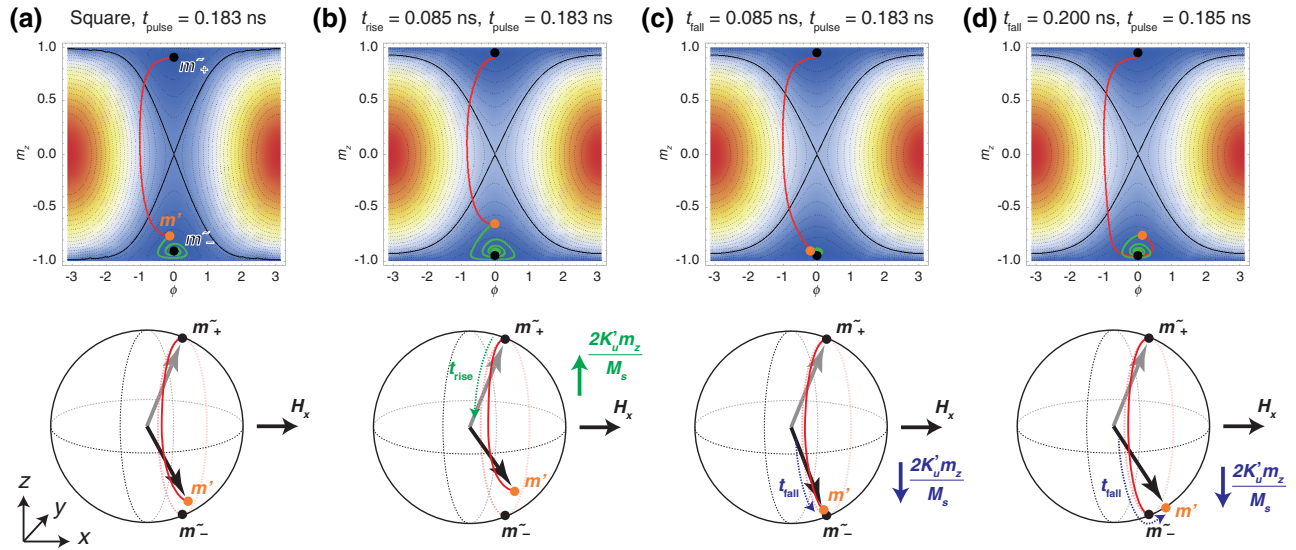


FIG. 4. Effects of t_{rise} and t_{fall} on magnetization trajectory. Red and green lines represent, respectively, the magnetization trajectory during and after t_{pulse} . Orange dots denote the magnetization direction at the end of the voltage pulse. Black dots around $m_z = +1$ and -1 denote \tilde{m}_+ and \tilde{m}_- , respectively. ϕ is the azimuth angle from the x direction in which a static magnetic field is applied. The panels at the bottom illustrate the relationship between the magnetization trajectory and the effective field.

other words, we would certainly obtain a WER of zero for these three cases regardless of the difference in the magnetization direction at the end of the voltage pulse (m'). However, when the temperature is raised, the magnetization trajectory deviates from the trajectory at $T = 0$ K and the magnetization switching becomes probabilistic. The probability that the switching will fail increases as m' gets higher magnetic energy.

An important thing to note is that, as displayed in Fig. 4(a), m' never reaches \tilde{m}_- or \tilde{m}_+ (which correspond to energy minima) whatever t_{pulse} is chosen as long as one uses square pulses. This is because, in the case of square voltage pulses, the magnetization merely precesses around H_x while undergoing magnetization damping. Therefore, the magnetization gradually gets closer to $m_x = 1$ as it undergoes precession during t_{pulse} . The situation is different

if nonzero t_{rise} and/or nonzero t_{fall} is introduced. During t_{rise} and t_{fall} , the magnetization is subjected not only to H_x but also to the anisotropy field due to uncompensated perpendicular magnetic anisotropy $K'_u(V, t)$, which is given by

$$H_{\text{ani}} = \frac{2K'_u m_z}{M_s}. \quad (4)$$

H_{ani} applies an additional torque on the magnetization that tilts m to H_x during t_{rise} , or pulls m away from H_x during t_{fall} , because H_{ani} changes its polarity according to the polarity of m_z . By our introducing $t_{\text{rise}} = 0.10$ ns [Fig. 4(b)], m' comes closer to the saddle point. On the other hand, as can be seen in Fig. 4(c), a proper t_{fall} can compensate for the shift of magnetization due to the

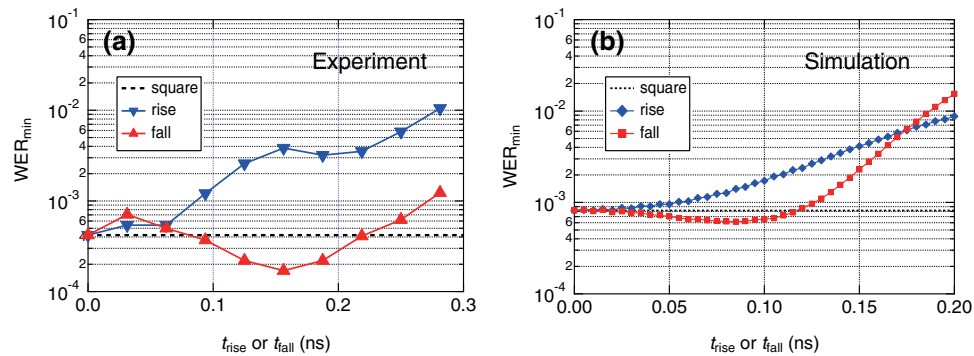


FIG. 5. Minimum value of the WER (WER_{min}) as a function of t_{rise} (blue symbols) and t_{fall} (red symbols): (a) experimental results; (b) numerical simulation results.

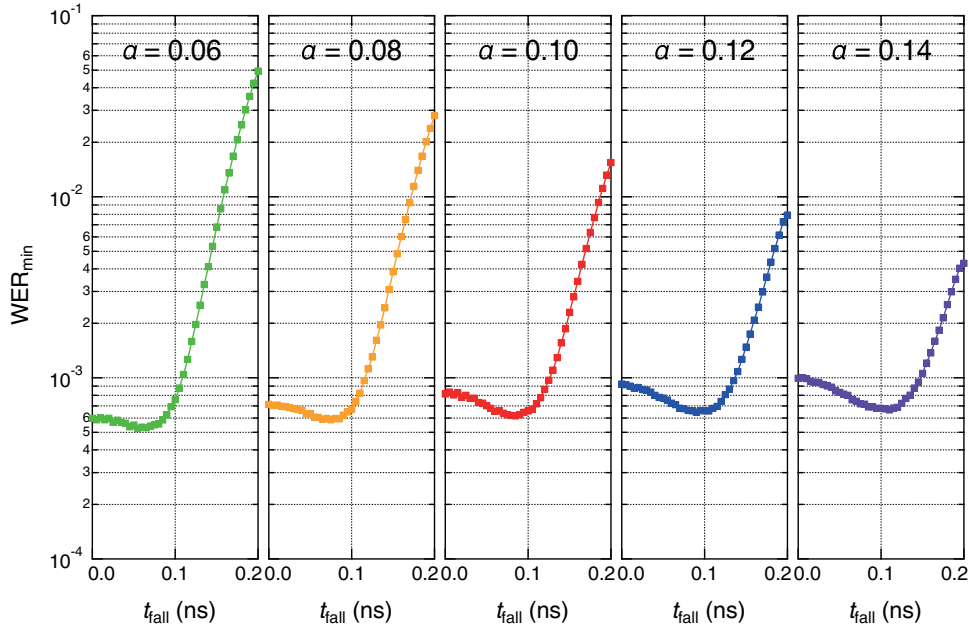


FIG. 6. Numerically simulated minimum value of the WER (WER_{\min}) as a function of t_{fall} for different α .

damping and one can deliver m' to \tilde{m}_- . The numerical simulations also explain the increase of the WER for large t_{fall} as observed in Figs. 3(d), 3(g), and 3(h). Figure 4(d) displays the magnetization trajectory for $t_{\text{fall}} = 0.2$ ns and $t_{\text{pulse}} = 0.215$ ns. Although the magnetization passes \tilde{m}_- during the pulse, \tilde{m}_- is *not* an energy minimum at that moment because of the remaining VCMA effect and m' ends up getting farther from \tilde{m}_- .

The above discussions are validated by the plot of the minimum value of the WER as a function of t_{rise} and t_{fall} . Figures 5(a) and 5(b) correspond, respectively, to the results obtained in experiments and numerical simulations that take the thermal effects ($T = 300$ K) into account. For both cases the minimum value of the WER increases almost monotonically as t_{rise} increases. However, the dependence of the minimum value of the WER on t_{fall} is nonmonotonic: the minimum value of the WER decreases when a small t_{fall} is introduced, and in the experiments the WER is a minimum at $t_{\text{fall}} = 0.156$ ns. The numerical simulation results are slightly different; in this case the minimum value of the WER is at $t_{\text{fall}} = 0.085$ ns. These results are in good accordance with the magnetization trajectory shown in Fig. 4(c) for which m' comes closest to \tilde{m}_- , thus further demonstrating the importance of precisely controlling magnetization to minimize the WER.

Finally, we show in Fig. 6 the influence of varying α on the WER reduction using pulse shaping. A similar WER reduction is obtained regardless of the α value by the application of a small t_{fall} . However, as shown in Fig. 7, t_{fall} at which the WER is a minimum becomes larger as α is increased. It is also important to note that the magnitude of the WER reduction becomes larger for larger α . This

shows that the present pulse-shaping method can effectively mitigate the write-error increase due to intrinsically nonzero α in ferromagnets.

IV. SUMMARY

To summarize, we investigate the effects of pulse shape on voltage-driven magnetization switching. We find that the minimum value of the WER monotonically increases as t_{rise} increases but is reduced when a small t_{fall} is introduced. The experimental results are reproduced well by the numerical simulations, and it is found that the dependence of the minimum value of the WER on t_{rise} and t_{fall} can be explained by magnetization-trajectory changes due to VCMA-induced inclination of the precession axis.

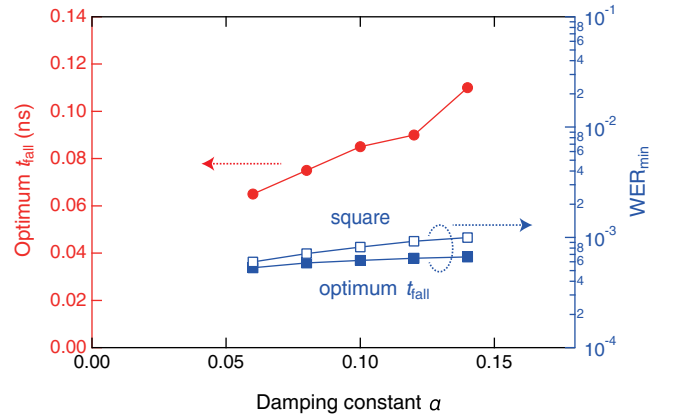


FIG. 7. Effects of pulse shaping for different α . WER_{\min} , minimum value of the WER.

This shows that the trajectory of precessing magnetization can be precisely manipulated by precisely controlling the voltage-pulse shape. It is noteworthy that simple numerical simulations based on the macrospin approximation successfully reproduce the experimental results. This indicates how useful numerical simulations are for understanding magnetization dynamics driven by pulsed voltage and also for finding methods of reducing the WER.

ACKNOWLEDGMENTS

The authors acknowledge T. Taniguchi, S. Tsunegi, and A. Sugihara for their fruitful discussions, and E. Usuda, and M. Toyoda for assisting with the experiments. This work was supported by the ImPACT Program of the Council for Science, Technology and Innovation.

-
- [1] T. Zhao, A. Scholl, F. Zavaliche, K. Lee, M. Barry, A. Doran, M. P. Cruz, Y. H. Chu, C. Ederer, N. A. Spaldin, R. R. Das, D. M. Kim, S. H. Baek, C. B. Eom, and R. Ramesh, Electrical control of antiferromagnetic domains in multiferroic BiFeO₃ films at room temperature, *Nat. Mater.* **5**, 823 (2006).
- [2] D. Lebeugle, A. Mougin, M. Viret, D. Colson, and L. Ranno, Electric Field Switching of the Magnetic Anisotropy of a Ferromagnetic Layer Exchange Coupled to the Multiferroic Compound BiFeO₃, *Phys. Rev. Lett.* **103**, 257601 (2009).
- [3] Y.-H. Chu, L. W. Martin, M. B. Holcomb, M. Gajek, S.-J. Han, Q. He, N. Balke, C.-H. Yang, D. Lee, W. Hu, Q. Zhan, P.-L. Yang, A. F.-Rodriguez, A. Scholl, S. X. Wang, and R. Ramesh, Electric-field control of local ferromagnetism using a magnetoelectric multiferroic, *Nat. Mater.* **7**, 478 (2008).
- [4] J. T. Heron, M. Trassin, K. Ashraf, M. Gajek, Q. He, S. Y. Yang, D. E. Nikonov, Y.-H. Chu, S. Salahuddin, and R. Ramesh, Electric-Field-Induced Magnetization Reversal in a Ferromagnet-Multiferroic Heterostructure, *Phys. Rev. Lett.* **107**, 217202 (2011).
- [5] M. Weisheit, S. Fähler, A. Marty, Y. Souche, C. Poinsignon, and D. Givord, Electric field-induced modification of magnetism in thin-film ferromagnets, *Science* **315**, 349 (2007).
- [6] T. Maruyama, Y. Shiota, T. Nozaki, K. Ohta, N. Toda, M. Mizuguchi, A. A. Tulapurkar, T. Shinjo, M. Shiraishi, S. Mizukami, Y. Ando, and Y. Suzuki, Large voltage-induced magnetic anisotropy change in a few atomic layers of iron, *Nat. Nanotech.* **4**, 158 (2009).
- [7] M. Endo, S. Kanai, S. Ikeda, F. Matsukura, and H. Ohno, Electric-field effects on thickness dependent magnetic anisotropy of sputtered MgO/Co₄₀Fe₄₀B₂₀/Ta structures, *Appl. Phys. Lett.* **96**, 212503 (2010).
- [8] D. Chiba, M. Sawicki, Y. Nishitani, Y. Nakatani, F. Matsukura, and H. Ohno, Magnetization vector manipulation by electric fields, *Nature* **455**, 515 (2008).
- [9] C. G. Duan, J. P. Velev, R. F. Sabirianov, Z. Zhu, J. Chu, S. S. Jaswal, and E. Y. Tsymbal, Surface Magnetoelectric Effect in Ferromagnetic Metal Films, *Phys. Rev. Lett.* **101**, 137201 (2008).
- [10] K. Nakamura, R. Shimabukuro, Y. Fujiwara, T. Akiyama, T. Ito, and A. J. Freeman, Giant Modification of the Magnetocrystalline Anisotropy in Transition-Metal Monolayers by an External Electric Field, *Phys. Rev. Lett.* **102**, 187201 (2009).
- [11] M. Tsujikawa, and T. Oda, Finite Electric Field Effects in the Large Perpendicular Magnetic Anisotropy Surface Pt/Fe/Pt(001): A First-Principles Study, *Phys. Rev. Lett.* **102**, 247203 (2009).
- [12] M. K. Niranjan, C.-G. Duan, S. S. Jaswal, and E. Y. Tsymbal, Electric field effect on magnetization at the Fe/MgO(001) interface, *Appl. Phys. Lett.* **96**, 222504 (2010).
- [13] S. Miwa, M. Suzuki, M. Tsujikawa, K. Matsuda, T. Nozaki, K. Tanaka, T. Tsukahara, K. Nawaoka, M. Goto, Y. Kotani, T. Ohkubo, F. Bonell, E. Tamura, K. Hono, T. Nakamura, M. Shirai, S. Yuasa, and Y. Suzuki, Voltage controlled interfacial magnetism through platinum orbits, *Nat. Commun.* **8**, 15848 (2017).
- [14] T. Nozaki, Y. Shiota, S. Miwa, S. Murakami, F. Bonell, S. Ishibashi, H. Kubota, K. Yakushiji, T. Saruya, A. Fukushima, S. Yuasa, T. Shinjo, and Y. Suzuki, Electric-field-induced ferromagnetic resonance excitation in an ultrathin ferromagnetic metal layer, *Nat. Phys.* **8**, 491 (2012).
- [15] J. Zhu, J. A. Katine, G. E. Rowlands, Y.-J. Chen, Z. Duan, J. G. Alzate, P. Upadhyaya, J. Langer, P. K. Amiri, K. L. Wang, and I. N. Krivorotov, Voltage-Induced Ferromagnetic Resonance in Magnetic Tunnel Junctions, *Phys. Rev. Lett.* **108**, 197203 (2012).
- [16] Y. Shiota, T. Nozaki, F. Bonell, S. Murakami, T. Shinjo, and Y. Suzuki, Induction of coherent magnetization switching in a few atomic layers of FeCo using voltage pulses, *Nat. Mater.* **11**, 39 (2012).
- [17] S. Kanai, M. Yamanouchi, S. Ikeda, Y. Nakatani, F. Matsukura, and H. Ohno, Electric field-induced magnetization reversal in a perpendicular-anisotropy CoFeB-MgO magnetic tunnel junction, *Appl. Phys. Lett.* **101**, 122403 (2012).
- [18] C. Grezes, F. Ebrahimi, J. G. Alzate, X. Cai, J. A. Katine, J. Langer, B. Ocker, P. K. Amiri, and K. L. Wang, Ultra-low switching energy and scaling in electric-field-controlled nanoscale magnetic tunnel junctions with high resistance-area product, *Appl. Phys. Lett.* **108**, 012403 (2016).
- [19] S. Kanai, F. Matsukura, and H. Ohno, Electric-field-induced magnetization switching in CoFeB/MgO magnetic tunnel junctions with high junction resistance, *Appl. Phys. Lett.* **108**, 192406 (2016).
- [20] Y. Shiota, T. Nozaki, S. Tamaru, K. Yakushiji, H. Kubota, A. Fukushima, S. Yuasa, and Y. Suzuki, Evaluation of write error rate for voltage-driven dynamic magnetization switching in magnetic tunnel junctions with perpendicular magnetization, *Appl. Phys. Express* **9**, 013001 (2016).
- [21] Y. Shiota, T. Nozaki, S. Tamaru, K. Yakushiji, H. Kubota, A. Fukushima, S. Yuasa, and Y. Suzuki, Reduction in write error rate of voltage-driven dynamic magnetization switching by improving thermal stability factor, *Appl. Phys. Lett.* **111**, 022408 (2017).

- [22] T. Yamamoto, T. Nozaki, Y. Shiota, H. Imamura, S. Tamaru, K. Yakushiji, H. Kubota, A. Fukushima, Y. Suzuki, and S. Yuasa, Thermally Induced Precession-Orbit Transition of Magnetization in Voltage-Driven Magnetization Switching, [Phys. Rev. Appl. **10**, 024004 \(2018\)](#).
- [23] S. Tamaru, T. Yamamoto, T. Nozaki, and S. Yuasa, Accurate calculation and shaping of the voltage pulse waveform applied to a voltage-controlled magnetic random access memory cell, [Jpn. J. Appl. Phys. **57**, 073002 \(2018\)](#).
- [24] W. F. Brown, Thermal fluctuations of a single-domain particle, [Phys. Rev. **130**, 1677 \(1963\)](#).